Journal of Materials Chemistry A

Accepted Manuscript

ROYAL SOCIETY OF CHEMISTRY

www.rsc.org/materialsA

A nanofibrous silver-nanoparticle/titania/carbon composite as anode material for lithium ion batteries

Shun Li and Jianguo Huang*

Department of Chemistry, Zhejiang University, Hangzhou, Zhejiang 310027, China
E-mail: jghuang@zju.edu.cn

Graphic Abstract Entry:

A nanofibrous silver-nanoparticle/titania/carbon Composite as anode material for lithium ion batteries

Shun Li and Jianguo Huang*

Nanofibrous Ag-NP/titania/carbon composite derived from cellulose substance was fabricated, showing enhanced electrochemical performances as anode material for LIBs.

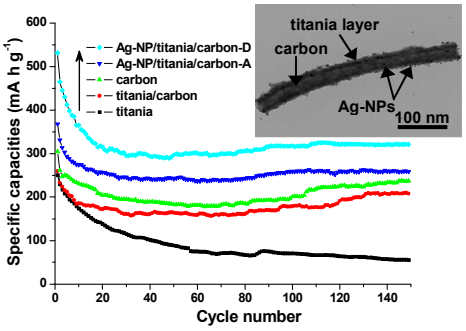

Journal of Materials Chemistry A

paper

Cite this: DOI: 10.1039/c0xx00000x

www.rsc.org/MaterialsB

A nanofibrous silver-nanoparticle/titania/carbon composite as anode material for lithium ion batteries†

Shun Li and Jianguo Huang*

Received (in XXX, XXX) Xth XXXXXXXXX 20XX, Accepted Xth XXXXXXXXX 20XX

DOI: 10.1039/b000000x

Deposition of silver nanoparticles (Ag-NPs) onto the surfaces of the titania/carbon nanocomposite fibres that fabricated by employing natural cellulose substance (commercial laboratory filter paper) as both scaffold and carbon source resulted in a new nanofibrous ternary Ag-NP/titania/carbon composite material, which was employed as anode material for lithium ion batteries showing improved electrochemical performances compared with the titania, carbon and titania/carbon hybrid counter materials. For such a composite with 22.48 wt.% of silver and sizes of the Ag-NPs of 5−10 nm, an initial discharge capacity was 1323 mA h g^{-1} at a current density of 100 mA g^{-1}, and showed a stable capacity of 320 mA h g^{-1} after 150 charge/discharge cycles. It was found that the electrochemical performances of the anode material get better with the increment of the silver content in the composites. Due to the enhanced electric conductivity caused by the silver nanoparticles, as well as the unique three-dimensional cross-linked networks structure of the composite, the anode performances in terms of the capacity, cycling stability and rate capacity are significantly improved.

Introduction

Lithium-ion batteries (LIBs) have been an attractive power resource in recent decades due to their high-energy density, large-scale energy storage capacity and the low-cost.[1–5] The electrochemical performances of LIBs are greatly affected by the anode and cathode materials employed, and much attention has been paid on the anode materials of which.[6,7] Carbon-based matters have been considered as the most optimal anode materials in LIBs due to their favorable cycling performances, low cost and safety.[8–10] However, carbonaceous materials were subjected to a number of serious disadvantages, such as low specific capacity (372 mA h g^{-1}), relatively higher charge lose due to the formation of the solid electrolyte interface (SEI) layers, and low lithium intercalation voltage (0−0.2 V *vs.* Li/Li^+). In order to overcome these shortcomings, alternatives like silicon- and tin-based materials have been adopted, while the electrochemical performances of which are suffered from the huge volume changes and the fast capacity decay during the electrochemical charge/discharge processes.[11,12] The challenges in using metal oxides as anode materials are their poor cycling performance, low electronic conductivity and volume expansion occurring during cycling.[13,14] Titanium dioxide (TiO_2) matters, due to their long cycle life, non-toxicity, environment friendliness and low cost, have been considered as anode materials for rechargeable lithium-ion batteries.[15,16] In particular, titania-based materials as anodes for LIBs show a comparatively high Li/Li^+ voltage at about 1.7 V,[17,18] which can effectively avoid the formation of the SEI layers. Titania matters with various nanoscale structures such as nanotubes,[19,20] nanoparticles[21,22] and nanowires[23] have demonstrated enhanced rate capabilities and cycling performances.[24] It has been shown that nanostructured titanium oxides can effectively shorten the diffusion path of Li^+ ions and the transportation of electrons,[25] which benefits the charge/discharge process and accommodates the volume expansion during the lithium insertion/extraction reactions. However, as an anode material for LIBs, poor electronic conductivity of titania (~10^{-12} Ω^{-1} cm^{-1}) has limited its practical applications.[26,27] To address the challenge, titania-based composites with different crystalline forms, morphologies and nanostructures have been fabricated and applied as anode materials of LIBs. Rahman and co-workers demonstrated that silver nanoparticle (Ag-NP) coated titania nanostructured anode materials showed better cyclic performance at 10 mA g^{-1};[28] and Li *et al.* reported Ag-NP modified titania nanotubes gave a capacity of 190 mA h g^{-1} after 40 charge/discharge cycles.[29] The Ag-NPs existing in the related composite materials are believed to improve the electrochemical performances of which, as reported by Maier *et al.*, Ag-NP coated three-dimensional macroporous silicon composite as electrodes not only improve the reversible capacity of 1163 mA h g^{-1} at a rate of 0.2 C after 100 cycles, but also enhance the rate capability of 1930 mA h g^{-1} (1 C).[30] And it was reported that silver-treated porous silicon particles as anode materials for LIBs have enhanced the conductivity of the composite.[31]

In the present work, by using natural cellulosic substances (common commercial laboratory filter paper) as both scaffold and carbon source, a new nanofibrous ternary Ag-NP/titania/carbon composite material was resulted, which was employed as anode material for LIBs showing enhanced electrochemical performance compared with the titania, carbon and titania/carbon

Department of Chemistry, Zhejiang University, Hangzhou, Zhejiang 310027, China. E-mail: jghuang@zju.edu.cn; Fax: +86-571-8795-1202; Tel: +86-571-8795-1202

† Electronic supplementary information (ESI) available: Characterizations and electrochemical performances of the related materials.

hybrid counter materials. The composites fabricated reserved the three-dimensional porous network structures of the original filter paper, which act as a buffer matrix for the volume changes of the anodes upon the charge/discharge cycles, and facilitate the effective contact of the electrolyte and the electrode as well. Due to the enhanced electric conductivity caused by the silver nanoparticles, as well as the unique three-dimensional cross-linked network structures with the synergistic effect of titania and carbon, the Ag-NP/titania/carbon composites exhibited improved electrochemical performances in terms of the capacity, cycling stability and rate capacity.

Experimental

Chemicals

Titanium(IV) *n*-butoxide [Ti(O^nBu)$_4$] and silver nitrate were purchased from Sigma-Aldrich and J&K Chemical Ltd., respectively. Ordinary filter paper (quantitative ashless) was bought from Hangzhou Xinhua Paper Industry Co. Ltd. (China). All the other chemicals were guaranteed reagents and were used without further purification. The water used in all relevant experiments was purified by using a Milli-Q Advantage A10 system (Millipore, Bedford, MA, USA) with resistivity higher than 18.2 MΩ cm.

Preparation of the Ag-NP/titania/carbon composite

In a representative process (Scheme 1), ultrathin titania gel film was firstly deposited onto each cellulose nanofibre of the common commercial filter paper by the surface sol–gel process according to our previous report.[32] The obtained titania/cellulose composite sheet was carbonized in argon at 450°C (heating rate 1°C min^{-1}) for 1 h to obtain the nanofibrous titania/carbon composite.[33] Silver nanoparticles were afterwards deposited onto each of the nanofibre of the titania/carbon composite using a photocatalytic reduction method.[34] A piece of the titania/carbon composite sheet (diameter 2 cm) was immersed in 20 mL of $AgNO_3$ solution with varied concentrations of 0.5 M, 1.0 M and 1.5 M (in ethanol–water, 1 : 1 v/v) respectively for 2 h at room temperature, or in 20 mL of 2.0 M $AgNO_3$ solution for 5 h at 40 °C, followed by thoroughly washing with deionized water and ethanol for 5 times. After being dried in vacuum oven overnight at 37 °C, the resultant composite sheets were subjected to mercury lamp irradiation (365 nm, 300 W) for 1 h, and Ag-NP deposited nanofibrous titania/carbon composites were obtained, the corresponding samples are designated as sample Ag-NP/titania/carbon-A, B, C and D, respectively. For comparisons, pure nanofibrous titania matter was obtained by calcination of the as-deposited titania/filter paper composite sheet in air for 6 h at 450 °C (heating rate 1 °C min^{-1}) to remove the filter paper, and nanofibrous titania/carbon composite sheet was obtained by carbonization of the as-deposited titania/filter paper composite sheet in argon for 1 h at 450 °C (heating rate 1 °C min^{-1}).

Determination of the silver content

To determine the silver content in the Ag-NP/titania/carbon composites, 10.0 mg of the sample was put into a flask, followed by adding 10 mL of nitric acid (16 M) and refluxing at 100 °C for 1 h to dissolve the silver component. The obtained mixture was then filtered and washed with Mill-Q water for 5-6 times, the filtrate was collected and diluted to 25.0 mL using Mill-Q water, and then subjected to atomic absorption spectrophotometry (AAS) measurement.

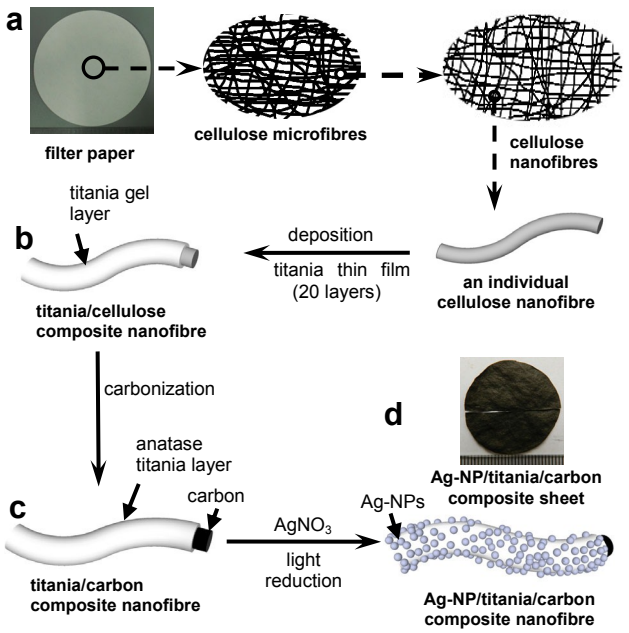

Scheme 1 Schematic illustration of the fabrication process of the nanotubular Ag-NP/titania/carbon composites derived from natural cellulose substance.

Electrochemical measurements

The working electrodes were made by mixing 80 wt.% active material with 10 wt.% acetylene black and 10 wt.% polyvinylidene fluoride binder in N-methyl-2-pyrrolidinone solvent to form a homogeneous slurry. The slurries were thereafter spread onto nickel foam, and the coated electrodes were dried in vacuum oven at 80 °C for 24 h and then pressed at the pressure of 10 atm. Subsequently, the standard CR2025 type coin cells were assembled in an Ar-filled glove box (O_2 < 0.1 ppm, H_2O < 0.1 ppm) using lithium metal foil as the counter electrode and polypropylene (PP) film as the separator. The electrolyte was 1.0 M $LiPF_6$ dissolved in a mixture of ethylene carbonate (EC) and dimethyl carbonate (DMC) with a volume ration of 1:1. Galvanostatic charge/discharge capacities were measured by cycling the half cells in the voltage range of 0.01−3 V *vs.* Li/Li$^+$. The battery performances were tested on a Neware battery testing system (Neware Technology Co., Ltd., Shenzhen, China) at room temperature. Cyclic voltammetry (CV) was carried out using a CHI760D electrochemical workstation system (CH instruments, Inc., China) with a scan rate of 0.1 mV s^{-1} between 0.01 and 3 V.

Characterization

Specimens for electron microscope examinations were prepared by sonication of the corresponding sample for about 60 s in ethanol, and drops of the resulted suspension were placed on silicon wafer or on carbon-coated copper grid followed by drying in air for field emission scanning electron microscopy (FE-SEM), transmission electron microscopy (TEM), and high resolution transmission electron microscopy (HR-TEM) observations, respectively. FE-SEM images were acquired on a Hitachi SU-70 electron microscope working at an accelerating voltage of 25.0 kV, and the specimens were sputtered with gold to increase the electrical conductivity. TEM and HRTEM characterizations were performed on a Hitachi HT-7700 microscope operating at an accelerating voltage of 100 kV and a Philips FEI Tecnai G2 F30 S-Twin microscope working at an accelerating voltage of 300 kV, respectively. X-ray diffraction (XRD) measurements were conducted on a Philips X'Pert PRO diffractometer with a $Cu_{K\alpha}$ (λ = 0.15405 nm) radiation source. X-ray photoelectron spectroscopy (XPS) was carried out using a VG Escalab Mark 2 spectrophotometer equipped with a $Mg_{K\alpha}$ X-ray source at energy of 1253.6 eV; high-resolution scans in the titanium, oxygen and silver regions were operated at 0.2 eV increments with a sweep time of 1000 ms eV^{-1} and 30 energy sweeps for each region. All of the binding energies were referenced to the C 1s peak at 284.50 eV. Atomic absorption spectroscopy (AAS) measurements were performed on Hitachi 180-50 spectrometer. Energy dispersive spectrometer measurement was tested on a HORIBA X-Max80006 instrument.

Results and discussion

Characterization of the Ag-NP/titania/carbon composite

The Ag-NP/titania/carbon composites fabricated exist as black free-standing bulk sheets (Scheme 1d), which is composed of titania thin layer coated carbon nanofibres with silver nanoparticles deposited on the surface. As mentioned in the experimental section, to control the density of the silver nanoparticles that deposited in the Ag-NP/titania/carbon composites, silver nitrate solutions with varied concentrations of 0.5 M, 1.0 M and 1.5 M were employed to fabricate samples A, B and C at room temperature; and 2.0 M silver nitrate solution was used to prepare sample D at a higher temperature of 40 °C to achieve higher silver loading. Fig. 1 shows the XRD diffraction patterns of samples B and D (samples A and C gave similar patterns), where the main diffraction peaks of silver nanoparticles are obviously observed. The peaks located at 2θ = 38.1°, 44.2°, 64.4° and 77.4° are attribute to (111), (200), (220), (311) reflection planes of Ag phase, respectively, which is in good consistent with the standard spectrum (JCPDS# 04-0783). With the density of the Ag-NP increases in the composites, the intensities of the anatase titania diffraction peak at 25.3° relatively decreases.[35] No obvious peaks corresponding to graphite carbon are found in the XRD pattern, which indicates that the carbon in the composite is in amorphous state.

Fig. 2a and b represents the FE-SEM images of sample Ag-NP/titania/carbon-D, it is seen that the initial network structures of the cellulose substance is reserved by which. It is composed of microfibre assemblies, and each microfibre is formed by

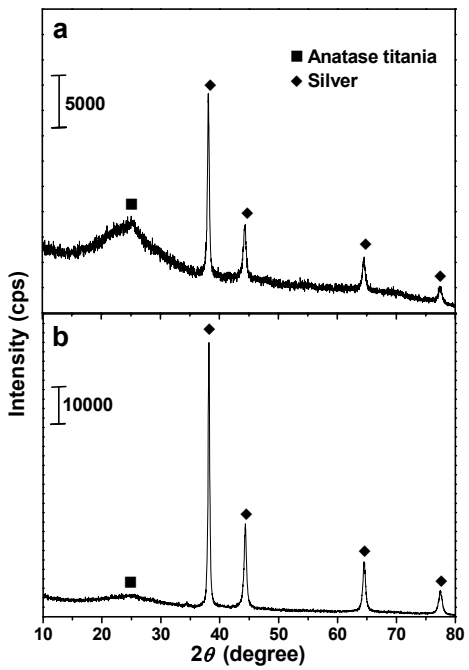

Fig. 1 X-ray diffraction patterns of samples Ag-NP/titania/carbon-B (curve a) and D (curve b).

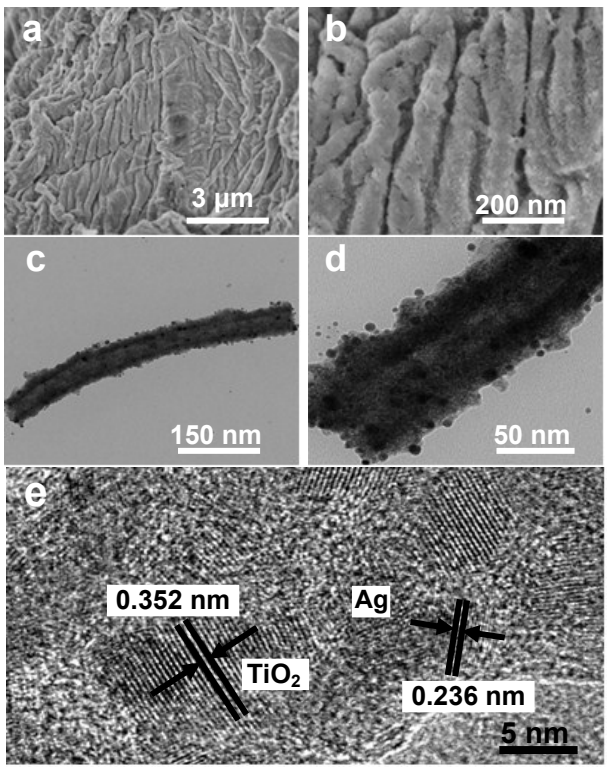

Fig. 2 Electron micrographs of the sample Ag-NP/titania/carbon-D (22.48 wt.% of silver). (a) and (b), FE-SEM images of the sample, showing nanofibre assemblies at different magnifications; (c) and (d), TEM micrographs of an individual Ag-NP/titania/carbon-D composite nanofrbre isolated from the nanofibre assemblies at different magnifications, and the diameter of which is about 100 nm, the size of the Ag-NPs is 5−10 nm; (e) HR-TEM image of the fibre surface, the lattice spacing of TiO_2 and Ag are 0.352 and 0.236 nm, respectively.

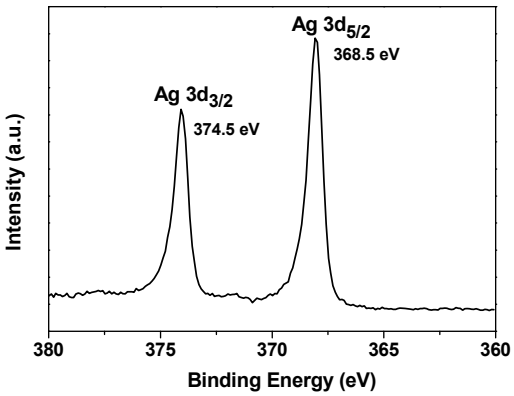

Fig. 3 The high-resolution XPS spectra of Ag 3d regions of sample Ag-NP/titania/carbon-D.

nanofibre assemblies. TEM micrographs shown in Fig. 2c and d indicate the cable structure of the composite nanofibre, the thin titania layer with a thickness about 10 nm is uniformly coated on the carbon nanofibre. Ag-NPs are deposited onto the titania/carbon composite nanofibre surface and the size of which is between 5 and 10 nm. Compared with Ag-NP/titania/carbon-D composite, the sizes of the silver nanoparticles in the samples Ag-NP/titania/carbon-A, B and C are smaller due to the lower concentration of the $AgNO_3$ solutions employed and the shorter immersion time at lower temperature (Fig. S1, S2 and S3, ESI†). The average diameters of the silver nanoparticles therein are 4−5, 5−6 and 6−8 nm, respectively. Moreover, the corresponding loading density of the silver nanoparticles in the samples increases follow the sequence of samples A to D, as indicated by the energy dispersive X-ray (EDX) results (Fig. S4, ESI†), which agrees well with the XRD results described above. To further clarify the structures of the composite nanofibres, the HR-TEM micrograph of sample Ag-NP/titania/carbon-D is displayed in Fig. 2e. The lattice spacings of 2.36 Å and 3.52 Å are distinctly observed, which correspond well to the lattice spacing of (111) plane of the cubic metallic silver phase and the (101) plane of anatase titania phase, respectively.

The chemical state of the silver component in sample Ag-NP/titania/carbon-D was determined by X-ray photoelectron spectroscopy (XPS), and the high-resolution spectrum of the Ag(3d) regions of the sample is shown in Fig. 3. The peaks located at 368.5 eV and 374.5 eV are indexed to the Ag $3d_{5/2}$ and Ag $3d_{3/2}$ of metallic silver, respectively, indicating that the silver nanoparticles deposited onto the surface of the titania/carbon nanofibre are in the metallic state.[36] The whole XPS spectra of sample Ag-NP/titania/carbon-D is shown in Fig. S5 (ESI†). For the titania component in the composite, the Ti(2p) doublet peak centered at 458.6 eV (Ti $2p_{3/2}$) and 464.6 eV (Ti $2p_{1/2}$) are observed, demonstrating the IV oxidation state of titanium.[37–40] The percentages of the silver contents in the Ag-NP/titania/carbon composites determined by AAS measurements are 9.27 wt%; 10.71 wt%; 11.87 wt% and 22.48 wt% for the samples A, B, C and D, respectively; indicating that the loading densities of the silver nanoparticles (as well as the sizes of which, as demonstrated by the TEM micrographs) in the composites can be effectively controlled by means of the current synthetic approach.

Electrochemical study of the Ag-NP/titania/carbon composite

The unique porous cross-linked three-dimensional structures of the present Ag-NP/titania/carbon composites that inherited from the initial cellulose substance scaffold would effectively relieve the severe volume change of the materials when served as anodes for LIBs, which is beneficial for the maintenance of the integrity of the electrodes. Moreover, the existing of the carbon nanofibres and the silver nanoparticles in the composites could facilitate the electron transfer during the charge/discharge processes of the batteries, resulting in better electrochemical performances.

The electrochemical performances of the Ag-NP/titania/carbon composites employed as anode materials of LIBs were investigated; and as comparisons, pure nanotubular anatase titania matter obtained by calcination of the as-prepared titania/filter paper composite sheets, carbon matter obtained by carbonization of filter paper, as well as anatase-titania/carbon composite produced by carbonization of the as-prepared titania/filter paper composite were used to assemble the LIBs to determine the corresponding electrochemical properties.

Fig. 4a shows the cyclic voltammetry curves of the Ag-NP/titania/carbon composites for the initial cycle in a voltage range between 0.01 and 3 V at a scan rate of 0.1 mV s^{-1}. A weak reduction peak was observed in the initial cathodic process, only a small peak at 0.6 V due to the electrochemical formation of amorphous Li_2O and the SEI layer was observed. In the anodic process, there is a broad weak peak between 1.0 and 1.75 V indicating the balance of Li^+ extraction, which is in accordance with the result of the charge/discharge profiles shown in Fig. 4b. Moreover, the redox peaks corresponding to TiO_2 is almost invisible in the curves due to the few content of which in the composite; and no relevant peaks are detected for the silver component, indicating that the Ag-NPs just act as an electronic additive in the electrode. The cyclic voltammetry curves of the titania, carbon and carbon/titania matters of the initial four cycles are shown in Fig. S6 (ESI†); for the pure nanotubular anatase titania, a pair of reduction/oxidation peaks at 1.7/2.2 V in the voltage range between 1 and 3 V at a scan rate of 0.1 mV s^{-1} are observed (Fig. S6a, ESI†), assigning to lithium-ion insertion/extraction in terms of anatase titania, which agrees well with the reported data.[25] The CV curves of the carbon and titania/carbon matters (Fig. S6b and c, ESI†) are similar as that of the Ag-NP/titania/carbon composites, and the reduction peaks shift to the higher voltage in the next three cycles and keep stable afterwards. This result indicates the irreversible phase transformation with the formation of the SEI layer in the first cycle; and suggests the good reversibility and structural stability of the electrode during the following lithium insertion/extraction processes.

Fig. 4b reveals the charge/discharge profiles of the sample Ag-NP/titania/carbon-D (22.48 wt.% of silver) at a current rate of 100 mA g^{-1} in the voltage range between 0.01 and 3 V. It possesses a specific capacity of 1323 mA h g^{-1} in the initial discharge cycle, which is much higher than those of the pure

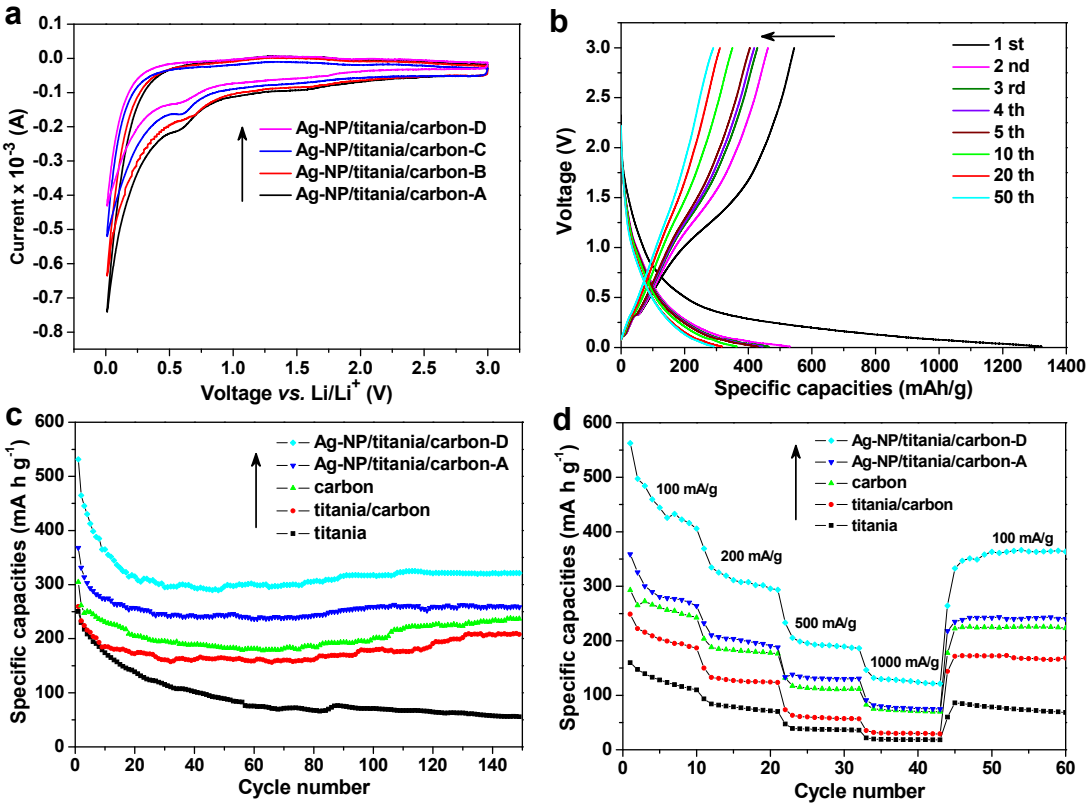

Fig. 4 Electrochemical performance of the Ag-NP/titania/carbon composites. (a) Cyclic voltammetry curves at a scan rate of 0.1 mV s^{-1} (voltage range: 0.01–3 V *vs.* Li/Li^+). (b) The charge–discharge profiles of sample Ag-NP/titania/carbon-D at 1st, 2nd, 3rd, 4th, 5th,10th, 20th and 50th cycle under a constant current density of 100 mA g^{-1} between 0.01 and 3.0 V. (c) The discharge cycling performance of the pure nanotubular titania matter, carbon matter obtained by carbonization of filter paper, titania/carbon composite, and samples Ag-NP/titania/carbon-A and D from the second cycle at the current densities of 100 mA g^{-1}. (d) The rate capabilities of the corresponding materials from the second cycle at various current densities.

nanotubular anatase titania (336 mA h g^{-1}), the carbon matter (837 mA h g^{-1}), and the titania/carbon composite (773 mA h g^{-1}); and is also higher than those of the samples Ag-NP/titania/carbon-A (9.27 wt.% of silver, 1081 mA h g^{-1}), B (10.71 wt.% of silver, 1055 mA h g^{-1}), and C (11.87 wt.% of silver, 1120 mA h g^{-1}) under the same experimental conditions (Fig. S7, ESI†). The initial charge specific capacity of sample Ag-NP/titania/carbon-D is 544 mA h g^{-1}, and the corresponding Coulombic efficiency is 41.1%. And a mild plateau between 1.0 and 1.75 V regions during the charge process is observed in the curves, which is identified as the lithium-ion extraction from the Li_xTiO_2. This irreversible capacity loss is due to the decomposition of the electrolyte. The Ag-NP/titania/carbon-D composite anode possess higher initial specific capacities (as compared with pure titania and carbon matters, the theoretical capacities of which are 335 and 372 mA h g^{-1}, respectively) and low Coulombic efficiency. This is due to the formation of the SEI layer and the decomposition of the nonaqueous electrolyte, and also caused by the existing of the carbon component in the composite. Similar results were observed for a sandwich structured graphene-based titania nanosheets which showed a first discharge capacity higher than the theoretical value of titania;[41] and a carbon/silicon nanocomposite which displayed a low initial Coulombic efficiency.[42] As revealed by the EDX measurement, the carbon content in the Ag-NP/titania/carbon-D composite is 56.62 wt% (Fig. S4, ESI†), the carbon nanofibres therein facilitate the charge transfer during the lithiation/delithiation processes. In the following charge/discharge cycles, the capacity of Ag-NP/titania/carbon-D composite decreases slightly; and the second charge/discharge specific capacity is 462 and 532 mA h g^{-1}, respectively, corresponding a Coulombic efficiency of 86.8%. The specific capacities in the next 3rd, 4th and 5th charge/discharge cycles are similar, the Coulombic efficiency in the 5th charge/discharge cycle reaches up to 94.2%; and a capacity of around 320 mA h g^{-1}after 150 cycles is still hold. As a comparison, the charge/discharge profiles of samples Ag-NP/titania/carbon-A, B and C at the 1st, 2nd, 3rd, 10th, 20th, and 50th cycle are shown in Fig. S7 (ESI†). It is found that the corresponding charge capacities in the initial cycle are 369, 364 and 410 mA h g^{-1}, with the Coulombic efficiencies of 34.1%, 34.5% and 36.6%, respectively; and at the 50th cycle, the corresponding discharge specific capacities are 243, 232, and 241 mA h g^{-1} for sample A, B and C, respectively. The differences in the specific capacities of the Ag-NP/titania/carbon composites are caused by the contents of metallic silver nanoparticles deposited therein. As indicated by the AAS results, sample D possess the

highest silver nanoparticle loading density, and sample A possess the lowest. It is clear that the higher loading density of the silver nanoparticles in the composites results in higher specific capacity of the anode. The existing of the silver nanoparticles in the composites is beneficial to acquire enhanced conductivity, and the three dimensional porous structures of the composites composed of anatase titania coated carbon nanofibres give a high specific surface area of the material, and the synergistic effect of carbon, titania and Ag-NPs facilitate the electron transportation, hence the electrochemical performances of the Ag-NP/titania/carbon composites are enhanced.

Fig. 4c displays the discharge cycling performances of the pure nanotubular anatase titania, carbon matter, titania/carbon composite and the samples Ag-NP/titania/carbon-A and D composite from the second cycle at the current densities of 100 mA g^{-1} at a voltage range between 0.01 and 3 V (except the titania case, which is 1−3 V). The capacities of all the materials decrease sharply within the first 10 cycles of charge/discharge processes, and reach a relatively stable value after 20 cycles except the titania matter. The capacity of the titania matter decreases slowly even after 150 cycles, and the corresponding capacity is about 50 mA h g^{-1}. The capacity of the carbon matter is higher than that of the titania/carbon composite, and slowly decreases to 200 mA h g^{-1} after 100 cycles, then gradually increased to nearly 250 mA h g^{-1} in the following 50 cycles. The capacity diversity between the titania/carbon composite and the carbon matter is due to the theoretical capacity of porous carbon (372 mA h g^{-1}) is larger than that of titania (335 mA h g^{-1}). As for the Ag-NP/titania/carbon composites, the cycling performances are greatly enhanced. Outstanding capacity retention of 326 and 252 mA h g^{-1} is achieved by samples Ag-NP/titania/carbon-D and A after 150 cycles, respectively (Fig. 4c); and the corresponding values are 276 and 290 mA h g^{-1} for samples B and C (Fig. S8a, ESI†). Compared with the titania-carbon/silver composite reported by Bhattacharyya *et al.* (with a first charge capacity of about 250 mA h g^{-1}),[36] and the Ag-NP/titania composite reported by Huang *et al.* (with a capacity of 120 mA g^{-1} after 20 cycles),[43] the present Ag-NP/titania/carbon-D composites show superior electrochemical behaviours. The improved electrochemical performances of the Ag-NP/titania/carbon composites are ascribed to the shorter lithium-ion diffusion route due to the fine nanostructures of the materials, improved electrode/electrolyte contact area resulted from the porous three-dimensional morphologies, as well as the enhanced conductivity resulted from the high loading density of the silver nanoparticles.

The rate performances of the related materials are displayed in Fig. 4d. For the Ag-NP/titania/carbon-D composite, at a current density of 100 mA g^{-1}, the discharge capacity sharply decreases in the first 10 cycles, while becomes relatively stable when cycled at higher currents; once the current goes back to 100 mA g^{-1}, the capacity partially recovers to the initial value, and 68.5% of the second cycle discharge capacity at 100 mA g^{-1} is recovered even after 150 cycles of charge/discharge processes. Compared with the results of the other four materials displayed in Fig. 4d, it is clear that the higher loading density of silver nanoparticles in the composite leads to improved specific capacity with good rate performances.

Conclusions

A new nanofibrous ternary Ag-NP/titania/carbon composite was fabricated by a facile approach using natural cellulose substance as scaffold and carbon source, which shows improved electrochemical performances as employed as anode materials of LIBs due to the unique three-dimensional porous structures of which, and the synergetic effect of the components. The current strategy provides a unique pathway for the development of bio-inspired nanomaterials aims at future energy applications. Biomimetic materials synthesis has been proven to be effective in the fabrication of materials with unique functionalities,[44–46] the introduction of the sophisticated structures of natural substances into energy-related artificial matters associated with further modifications would give new aspects in the design of electrode materials towards the development of high-performance lithium-ion batteries.

Acknowledgements

This work was supported by the National Natural Science Foundation of China (21173192).

Notes and references

1 P. G. Bruce, B. Scrosati and J. M. Tarascon, *Angew. Chem.*, *Int. Ed.*, 2008, **47**, 2930; and references therein.
2 J.-M. Tarascon and M. Armand, *Nature*, 2000, **414**, 359.
3 L. Kavan, J. Rathousky, M. Grätzel, V. Shklover and A. Zukal, *J. Phys. Chem. B*, 2000, **104**, 12012.
4 J. S. Chen and X. W. Lou, *Small*, 2013, **9**, 1877.
5 J. Jiang, Y. Li, J. Liu, X. Huang, C. Yuan and X. W. Lou, *Adv. Mater.*, 2012, **24**, 5166.
6 W.-M. Zhang, J.-S. Hu, Y.-G. Guo, S.-F. Zheng, L.-S. Zhong, W.-G. Song and L.-J. Wan, *Adv. Mater.*, 2008, **20**, 1160.
7 L. Ji, Z. Lin, M. Alcoutlabi and X. Zhang, *Energy Environ. Sci.*, 2011, **4**, 2682.
8 H. K. Liu, Z. P. Guo, J. Z. Wang and K. Konstantinov, *J. Mater. Chem.*, 2010, **20**, 10055.
9 S. W. Lee, N. Yabuuchi, Betar M. Gallant, S. Chen, B.-S. Kim, P. T. Hammond and Y. S.-Horn. *Nature Nanotech.*, 2010, **116**, 531.
10 M. Yoshio, H. Wang, K. Fukuda, Y. Hara and Y. Adachi, *J. Electrochem. Soc.*, 2000, **147**, 1245.
11 R. Teki, M. K. Datta, P. Krishnan, T. C. Parker, T. M. Lu, P. N. Kumta and N. Koratkar, *Small*, 2009, **5**, 2236.
12 A. D. W. Todd, P. P. Ferguson, M. D. Fleischauer and J. R. Dahn, *Int. J. Energy Res.*, 2010, **34**, 535.
13 T. D. Hatchard and J. R. Dahn, *J. Electrochem. Soc.*, 2004, **151,** A838.
14 M. Winter and J. O. Besenhard, *Electrochim Acta.*, 1999, **45**, 31.
15 H. S. Zhou, D. L. Li, M. Hibino and I. Honma, *Angew. Chem.*, *Int. Ed.*, 2005, **44**, 797.
16 L. Kavan, M. Kalbac, M. Zukalova, I. Exnar, V. Lorenzen, R. Nesper and M. Grätzel, *Chem. Mater.*, 2004, **16**, 477.
17 Y. S. Hu, L. Kienle, Y. G. Guo and J. Maier, *Adv. Mater.*, 2006, **18** ,1421.
18 Y. G. Guo, Y. S. Hu, W. Sigle and J. Maier, *Adv. Mater.*, 2007, **19**, 2087.
19 Y. Jiao, F. Chen, L. Zhang, E. Zhou and J. Zhang, *Catal. Commun.*, 2014, **47**, 32.
20 J. Xu, C. Jia, B. Cao and W. Zhang, *Electrochim. Acta*, *2007,* **52**, 8044.

21 S. W. Oh, S. Park and Y. Sun, *J. Power Sources*, 2006, **161**, 1314.
22 C. Jiang, I. Honma, T. Kudo and H. Zhou, *Electrochem. Solid-State Lett.*, 2007, **10**, A127.
23 Y. Wang, M. Wu and W. Zhang, *Electrochim. Acta*, 2008, **53,** 7863.
24 K. Wang, M. Wei, M. A. Morris, H. Zhou and J. D. Holmes, *Adv. Mater*, 2007, **19**, 3016.
25 Z. Yang, G. Du, Q. Meng, Z. Guo, X. Yu, Z. Chen, T. Guo and R. Zeng, *J. Mater. Chem.*, 2012, **22**, 5848.
26 I. Abayev, A. Zaban, F. Fabregat-Santiago and J. Bisquert, J. *Phys. Stat. Sol. A*, 2003, **196**, R4.
27 S. Yoon, B. H. Ka, C. Lee, M. Park and S. M. Oh, *Electrochem. Solid-State Lett.*, 2009, **12**, A28.
28 M. M. Rahman, J. Wang, D. Wexler, Y. Zhang, X. Li, S. Chou and H. Liu, *J. Solid-State Electrochem.*, 2010, **14**, 571.
29 B.-L. He, B. Dong and H.-L. Li, *Electochem. Commun.*, 2007, **9**, 425.
30 Y. Yu, L. Gu, C. Zhu, S. Tsukimoto, P. A. Aken and J. Maier, *Adv. Mater.*, 2010, **22**, 2247.
31 D. Chen, X. Mei, G. Ji, M, Lu, J. Xie, J. Lu and J. Y. Lee, *Adv. Mater.*, 2012, **51**, 2409.
32 J. Huang and T. Kunitake, *J. Am. Chem. Soc.*, 2003, **125**, 11834.
33 X. Liu, Y. Gu and J. Huang, *Chem. Eur. J.*, 2010, **16**, 7730.
34 X. Liu, Y. Luo, T. Wu and J. Huang, *New J. Chem.*, 2012, **36**, 2568.
35 P. A. A. P. Marques, T. Trindade and C. P. Neto, *Compos. Sci. Technol.*, 2006, **66**, 1038.
36 S. K. Das and A. J. Bhattacharyya, *Mater. Chem. Phys.*, 2011, **130**, 569.
37 M. Adler, B. Laughlin and S. G. Lieb, *Phys. Chem. Chem. Phys.*, 1999, **1**, 5327.
38 C.-T. Hsieh, I.-L. Chen, Y.-R. Jiang and J.-Y. Lin, *Solid State Ionics*, 2011, **201**, 60.
39 Y. Zhao, G. Liu, L. Liu and Z. Jiang, *J. Solid State Electrochem.*, 2009, **13**, 705.
40 A. Sivashanmugam, S. Gopukumar, R. Thirunakaran, C. Nithya and S. Prema, *Mater. Res. Bull.*, 2011, **46**, 492.
41 S. Yang, X. Fang and K. Müllen, *Adv. Mater.*, 2011, **23**, 3575.
42 S.-H. Ng, J. Wang, D. Welex, K. Konstantinov, Z.-P. Guo and H.-K. Liu. *Angew. Chem.*, *Int. Ed.*, 2006, **46**, 6898.
43 D. Fang, K. Huang, S. Liu and Z. Li, *J. Alloy Compd.*, 2008, **464**, L5.
44 J. Li, H. Möhwald, Z. An and G. Lu, *Soft Matt.*, 2005, **1**, 259.
45 Z. An, H. Möhwald, J. Li, *Biomacromolecules*, 2006, **7**, 580.
46 Q. He, Y. Cui, J. Li, *Chem. Soc. Rev.*, 2009, **38**, 2292.